

The structure of a *Burkholderia pseudomallei* immunophilin–inhibitor complex reveals new approaches to antimicrobial development

Isobel H. NORVILLE*†, Katherine O'SHEA*†, Mitali SARKAR-TYSON†, Suxin ZHENG‡, Richard W. TITBALL*, Gabriele VARANI‡¹ and Nicholas J. HARMER*¹

*School of Biosciences, University of Exeter, Geoffrey Pope Building, Stocker Road, Exeter EX4 4QD, U.K., †Defence Science and Technology Laboratory, Porton Down, Salisbury, Wiltshire SP4 0JQ, U.K., and ‡Departments of Chemistry and Biochemistry, University of Washington, Box 351700, Seattle, WA 98195-1700, U.S.A.

Mips (macrophage infectivity potentiators) are a subset of immunophilins associated with virulence in a range of micro-organisms. These proteins possess peptidylprolyl isomerase activity and are inhibited by drugs including rapamycin and tacrolimus. We determined the structure of the Mip homologue [BpML1 (*Burkholderia pseudomallei* Mip-like protein 1)] from the human pathogen and biowarfare threat *B. pseudomallei* by NMR and X-ray crystallography. The crystal structure suggests that key catalytic residues in the BpML1 active site have unexpected conformational flexibility consistent with a role in catalysis. The structure further revealed BpML1 binding to a helical peptide, in a manner resembling the physiological interaction of human TGF β RI (transforming growth factor β receptor I) with the human immunophilin FKBP12 (FK506-

binding protein 12). Furthermore, the structure of BpML1 bound to the class inhibitor cycloheximide *N*-ethylethanoate showed that this inhibitor mimics such a helical peptide, in contrast with the extended prolyl-peptide mimicking shown by inhibitors such as tacrolimus. We suggest that Mips, and potentially other bacterial immunophilins, participate in protein–protein interactions in addition to their peptidylprolyl isomerase activity, and that some roles of Mip proteins in virulence are independent of their peptidylprolyl isomerase activity.

Key words: *Burkholderia pseudomallei*, NMR, peptidylprolyl isomerase, small-molecule inhibitor, X-ray crystallography.

INTRODUCTION

Melioidosis is a community-acquired infection frequent in South-East Asia and Northern Australia [1]. Caused by the Gram-negative bacterium *Burkholderia pseudomallei*, the disease can range from a localized infection to an acute systemic, chronic or persistent disease. The symptoms of infection are diverse, often resembling tuberculosis or cancer. Consequently, the disease is likely to be often misdiagnosed [2]. The disease is especially pernicious as the bacterium is intrinsically resistant to a wide range of antibiotics [3]; even with optimal treatment, mortality in acute cases of disease ranges from 20 to 40% [2]. *B. pseudomallei* is also a potential bioterror agent [4]. Consequently, there has been a recent and concerted effort to develop novel countermeasures against this organism.

One potential target class for novel antimicrobials is the FKBP (FK506-binding proteins; tacrolimus). These ubiquitous enzymes catalyse the isomerization of pre-proline peptide bonds between the *cis* and *trans* configurations {PPIase (peptidylprolyl isomerase) activity [5]}, and form part of the broader category of PPIase enzymes. Several FKBP have been found to play a role in virulence in a range of species, including the bacteria *Legionella pneumophila* [6], *Chlamydia trachomatis* [7] and *Neisseria gonorrhoeae* [8], and the protozoan *Trypanosoma cruzi* [9]. One of the first bacterial FKBP to be studied in detail is a *L. pneumophila* protein required for the efficient invasion of macrophages [6]. Consequently, these proteins were labelled as

Mip (macrophage infectivity potentiator) proteins. The FKBP domain of the LpMip (*L. pneumophila* Mip) is required for virulence, and both antibodies binding to the active site and specific inhibitors sufficed to reduce the capacity of *Legionella* to invade macrophages [10,11]. We recently showed that a Mip-like protein from *B. pseudomallei*, BPSS1823 [hereafter BpML1 (*B. pseudomallei* Mip-like protein 1)], has high PPIase activity; and that it is required for efficient invasion of host cells and virulence in a mouse model of infection. Deletion of this gene significantly attenuates *B. pseudomallei* (I.H. Norville, N.J. Harmer, S. Harding, G. Fischer, K. Keith, K. Brown, M. Sarkar-Tyson and R.W. Titball, unpublished work).

Despite extensive study of Mips in a range of micro-organisms, the true biological targets for these proteins have not been clearly elucidated [8,11,12]. It has been broadly assumed that they act solely as isomerases [11]. Mips have been suggested to be an attractive target class for antimicrobials: there are known high-affinity inhibitors, indicating that the proteins are eminently druggable; and their prokaryotic functions are differentiated from those of higher eukaryotic FKBP.

We have previously shown that the BpML1 plays a key role in disease progression. In the present study, we report the molecular structure of BpML1, identify common features with other Mips and highlight differences from mammalian FKBP that could be exploited for drug design. We also identify new approaches to the design of compounds able to block this target. These compounds could be developed as antimicrobials to treat melioidosis, but

Abbreviations used: BpML1, *Burkholderia pseudomallei* Mip-like protein 1; FKBP, FK506-binding protein; HSQC, heteronuclear single-quantum coherence; LpMip, *Legionella pneumophila* Mip; Mip, macrophage infectivity potentiator; NOE, nuclear Overhauser effect; PPIase, peptidylprolyl isomerase; TGF β RI, transforming growth factor β receptor I.

¹ Correspondence may be addressed to either of these authors (email varani@chem.washington.edu or N.J.Harmer@exeter.ac.uk).

The structural co-ordinates reported for *Burkholderia pseudomallei* peptidylprolyl *cis*–*trans* isomerase, *B. pseudomallei* peptidylprolyl *cis*–*trans* isomerase in complex with cycloheximide *N*-ethylethanoate and BPSS1823, a *B. pseudomallei* Mip-like chaperone, have been deposited in the PDB under codes 2KE0, 2K07 and 2Y78 respectively.

could also have a much wider utility to treat other diseases where Mips play a key role in infection.

MATERIALS AND METHODS

Preparation of BpML1

Full-length BpML1 from *B. pseudomallei* strain K96243 was cloned into pET15b using the NdeI and HindIII sites. The vector was transformed into BL21 (DE3) cells. For enzymology, cells were grown in Luria-Bertani medium at 37°C with agitation until the D_{600} (attenuance at 600 nm) reached 0.4–0.6. IPTG (isopropyl β -D-thiogalactoside) was added to 1 mM and growth continued at 20°C for 4 h. Harvested cells were resuspended in 10 mM PBS supplemented with 100 mg/ml DNase I and Complete™ EDTA-free protease inhibitors (Roche), and disrupted by sonication. Clarified lysate was loaded on to a 1 ml Histrap FF column (GE Healthcare) and the recombinant protein was eluted in 10 mM PBS supplemented with 100 mM imidazole. The purified protein was dialysed against 10 mM PBS and samples frozen at –80°C until use. The protein concentration was determined using a bicinchoninic acid assay (Pierce Biotechnology).

For crystallization, cells were grown in ZYM-5052 medium [13] supplemented with 100 μ g/ml ampicillin at 37°C until the D_{600} was 0.5, and then at 20°C for 16 h. Harvested cells were resuspended in 20 mM Tris/HCl, pH 8.0 and 0.5 M NaCl (Buffer A), and lysed using a Soniprep 150 sonicator (MSE). Clarified lysate was purified using a nickel–agarose column (Bioline). Briefly, the loaded protein was washed with Buffer A supplemented with 20 mM imidazole-HCl (pH 8.0), and eluted with Buffer A supplemented with 250 mM imidazole-HCl (pH 8.0). BpML1 was then loaded on to a Superdex 200 16/60 hr column (GE Healthcare), and eluted isocratically with 10 mM Hepes (pH 7.0) and 0.5 M NaCl.

For NMR studies, 15 N-labelled and 13 C 15 N-labelled proteins were made by substituting 15 NH $_4$ Cl and/or [13 C]glucose for their unlabelled equivalents in the cell growth medium. 15 N-labelled and 13 C 15 N double-labelled proteins were dialysed into 20 mM potassium phosphate (pH 7.0), 100 mM KCl and 2 mM DTT (dithiothreitol), to a final protein concentration of approx. 1 mM. Cycloheximide *N*-ethylethanoate (>95%) was purchased from Life Chemicals without further purification. Samples of the complex were prepared by titrating unlabelled cycloheximide *N*-ethylethanoate into labelled protein samples while monitoring 15 N HSQC (heteronuclear single-quantum coherence) chemical shift changes until a previously established ‘saturated’ spectrum was obtained.

Crystallization and structure solution

All crystals were grown using the microbatch method, and were prepared using an Oryx6 crystallization robot (Douglas Instruments). BpML1 at 14 mg/ml was mixed with an equal volume of 2.2 M (NH $_4$) $_2$ SO $_4$ and 0.1 M Bis/Tris (pH 5.5), and grown at 20°C. Prior to flash-freezing in liquid nitrogen, crystals were soaked for 30–60 s in a cryoprotectant solution of 1.1 M (NH $_4$) $_2$ SO $_4$, 0.1 M Bis/Tris (pH 5.5) and 30% (v/v) glycerol. Single-wavelength X-ray diffraction data were collected at a wavelength of 0.861 Å (1 Å = 0.1 nm) at 100 K at beamline I03 of the Diamond synchrotron (Table 1). Data were processed using iMOSFLM version 1.0.3 [14] and SCALA [15]. Initial phases were determined by molecular replacement using the structures of human FKBP12 (PDB code 1FKB) and the N-terminal

Table 1 Data collection and refinement statistics

Values in parentheses are for the highest-resolution shell.

	BpML1 (PDB code 2Y78)
Data collection	
Space group	$P4_32_12$
Cell dimensions*	
<i>a</i> , <i>b</i> , <i>c</i> (Å)	54.68, 54.68, 119.2
α , β , γ (°)	90, 90, 90
Resolution (Å)	40.3–0.91 (0.96–0.91)
R_{merge}	0.080 (0.398)
$I/\sigma I$	13.8 (2.2)
Completeness (%)	98.3 (88.2)
Redundancy	5.9 (2.7)
Refinement	
Resolution (Å)	40.3–0.91
Number of reflections	125 244
$R_{\text{work}}/R_{\text{free}}$	0.109/0.116
Number of atoms	
Protein	2032
Ligand/ion	58
Water	275
<i>B</i> -factors	
Protein	12.7
Ligand/ion	27.2
Water	24.2
Root mean square deviations	
Bond lengths (Å)	0.014
Bond angles (°)	1.586

*All data were collected from one crystal. High- and low-resolution passes were merged.

domain of rabbit FKBP59 (PDB code 1ROT) as a model. These structures were modified to remove non-homologous side chains using CHAINSAW [16]. Molecular replacement was performed using PHASER [17]. One protomer was observed in the asymmetric unit. Model building and refinement of the structures were performed using Coot version 0.6.1 [18] and PHENIX version 1.6.1 [19]. The structure was solved using anisotropic *B*-factors for all heavy atoms, riding hydrogen atoms, and optimization of stereochemical and ADP restraints. Structures were validated using PHENIX, Coot and MOLPROBITY [20]. The Ramachandran plot for the final model showed 100% of residues in the favoured region. Structural images were prepared using the PyMOL molecular graphics system, version 1.3 (Schrödinger).

NMR structure solution

All NMR spectra were collected at 298 K. 15 N HSQC, triple-resonance spectroscopy, HCCH TOCSY [21], three-dimensional 15 N-edited NOESY and three-dimensional 13 C-edited NOESY [22] were recorded on a Bruker Avance 500-MHz spectrometer with a cryoprobe. The two-dimensional ^1H - ^1H NOESY and ^1H - ^1H TOCSY spectra were recorded on a Bruker Avance 750-MHz spectrometer. Backbone resonance assignments of H, N, C $_{\alpha}$, C', and side-chain C $_{\beta}$ were performed using triple-resonance HNCA [23], CBCA(CO)NH [24], HNCACB and HN(CO)CA. The remaining side-chain resonance assignments were obtained from the analysis of 15 N-edited NOESY, 13 C-edited NOESY and HCCH-TOCSY spectra. Aromatic ring protons and protected amides were identified from two-dimensional ^1H - ^1H NOESY, ^1H - ^1H TOCSY and 15 N HSQC respectively collected from a sample exchanged into a 100% $^2\text{H}_2\text{O}$ NMR buffer. The assignments

of the ligand were obtained based on the two-dimensional ^{13}C -filtered NOESY and TOCSY spectra of the 'F1fF2f' type [25]. The two-dimensional ^{13}C - ^{12}C NOESY spectra were collected to facilitate the assignments of protein–ligand intermolecular NOEs (nuclear Overhauser effects) [26].

Spectral data were processed using NMRPipe [27] and analysed using CcpNmr Analysis 1.0 [28]. The structure calculations were conducted automatically by CYANA2.1 [29,30] based on NOEs selected from ^{15}N -edited NOESY, ^{13}C -edited NOESY, ^1H - ^1H NOESY and ^{13}C - ^{12}C NOESY, as well as additional dihedral-angle and hydrogen-bond constraints generated from the NMR data.

Inhibitor assay

PPIase activity of BpML1 protein was determined by a protease-coupled assay as described previously [31]. Briefly, 10 nM BpML1 protein was incubated for 6 min at 6°C in 1.2 ml of 35 mM Hepes buffer, pH 7.8 with succinyl-Ala-Phe-Pro-Phe-*p*-nitroanilide (10 mg/ml; Bachem). α -chymotrypsin (Sigma) was added to the cuvette to a final concentration of 1.25 mg/ml and mixed. Hydrolysis of the substrate was measured at 390 nm using a Shimadzu 1800 UV–visible spectrophotometer at 1 s intervals until there was no further change in absorbance. For inhibition measurements, BpML1 protein was pre-incubated with various concentrations of cycloheximide-*N*-ethylethanoate from 1 to 500 μM for 6 min prior to addition of chymotrypsin. At least three independent readings were taken at each data point. All data fitting and statistical analyses were performed using SPSS v16.0 (IBM). The pseudo first-order rate constant was calculated using eqn (1) [32]; data from 10 to 50 s (following the lag phase, and before substrate became limiting) were taken, and k_{obs} was calculated by linear regression.

$$\ln[A_{\infty} - A_t] = -k_{\text{obs}}t + \ln[A_{\infty} - A_0] \quad (1)$$

The enzymatic rate was determined by comparing the observed rate with the uncatalysed rate (eqn 2):

$$k_{\text{enz}} = k_{\text{obs}} - k_{\text{uncat}} \quad (2)$$

Data for inhibitor assays were fitted to eqn (3) [33] using least squares non-linear fitting. $[\text{E}]$ was treated as a constant (10 nM); v_0 and K_1^{app} were fitted, using initial estimates based on the raw data.

$$v = v_0 \frac{[\text{E}] - [\text{I}] - K + \sqrt{([\text{E}] - [\text{I}] - K)^2 + 4[\text{E}]K}}{2[\text{E}]} \quad (3)$$

RESULTS AND DISCUSSION

The BpML1 fold and active-site residue configuration are highly similar to LpMip

We solved the X-ray structure of BpML1 to 0.91 Å (Table 1). The structure confirmed that BpML1 adopts a classical FKBP fold (Figure 1A). Closer inspection of the active site in the crystal revealed that key side chains adopt a conformation that closely resembles that of the ligand-free *L. pneumophila* Mip FKBP domain (Figure 1B). NMR structures of BpML1 that were determined independently show an excellent similarity in overall fold with the crystal structure. They also demonstrate that there is considerable flexibility in both

Table 2 NMR and refinement statistics

Parameter	Apo-BpML1 (PDB code 2KE0)	BpML1–CNE complex (PDB code 2K07)
Structure constraints		
Distance constraints*		
Total meaningful NOE	1792	1757
Restraints		
Short range ($ i-j \leq 1$)	777	808
Medium range ($1 < i-j < 5$)	216	205
Long range ($ i-j \geq 5$)	799	744
Hydrogen-bond restraints	78	92
Dihedral angle restraints (ϕ, ψ)†	134	136
Total number of constraints	2004	1985
Constraints per residue	17.1	16.8
Intermolecular NOE restraints		
		39
Residual constraint violations‡		
CYANA target function	0.84	1.54
Distance violations (> 0.2 Å)	3	4
Torsion angles ($> 5.0^\circ$)	0	0
Ramachandran statistics (%)§		
Favoured	80.8	80.7
Additionally allowed	19.0	19.0
Generously allowed	0.1	0.3
Disallowed	0.0	0.0
Average root mean square deviation to the mean (Å)		
Backbone	0.39 ± 0.05	0.52 ± 0.15
Heavy atom	0.89 ± 0.08	0.98 ± 0.15
Ligand heavy atom		1.11 ± 0.14

*Final 20/100 structures selected based on the lowest CYANA target function.

†Dihedral angle restraints derived from TALOS [47].

‡Maximum violation shown in parentheses.

§Ramachandran analysis was performed with PROCHECKNMR.

||The average root mean square deviation to the mean of the protein was calculated over regions 13–117.

peripheral loops and side chains (Figure 1C) in the well-defined active site (see Supplementary Figure S1 available at <http://www.BiochemJ.org/bj/437/bj4370413add.htm> [34,35]). In particular, the $\beta 4$ – $\beta 5$ loop, which contributes the key Tyr⁸⁹ side chain to the active site, shows two distinct conformations in solution; and several of the key conserved active-site side chains have considerable flexibility. These observations are in contrast with Mip from *L. pneumophila* and *T. cruzi*, which show a remarkable commonality in the conformations adopted by these regions (see Supplementary Figure S2 available at <http://www.BiochemJ.org/bj/437/bj4370413add.htm> [34,36,37]). These observations suggest that previous structures (especially crystal structures) might be trapping a preferred low-energy conformation that may be catalytically relevant, but which does not capture the full range of dynamics available to the enzyme in solution.

BpML1 forms protein–protein interactions reminiscent of other FKBP

The protein sample used for crystallization of BpML1 had been cloned with a His₆ tag, linked to the protein by a thrombin cleavage site (sequence MSSHHHHHHSSGLVPRGSHM..., thrombin site underlined). The thrombin cleavage peptide was clearly resolved in the electron density, and forms an interaction with a neighbouring molecule in the crystal. This interaction placed the peptide directly in the active site of the neighbouring molecule, forming an apparently tight interaction, burying 890 Å² of surface

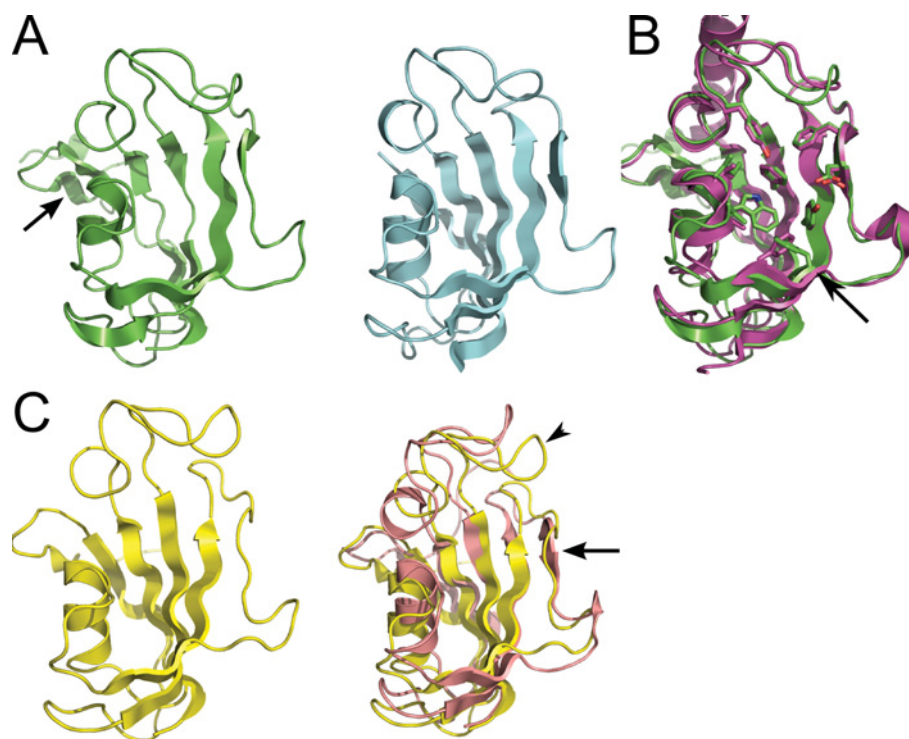


Figure 1 Structures of BpML1

(A) Cartoon of the 0.91 Å structure of BpML1 (left, green; PDB code 2Y78) compared with hFKBP12 (right, cyan; PDB code 2DG3 [48]). The overall fold is identical, with BpML1 containing all of the secondary structural elements, and an additional N-terminal β -strand (arrowed). (B) BpML1 shows an active-site conformation nearly identical with that of LpMip (purple; PDB code 1FD9). All of the most conserved side chains are identical in conformation, except for Phe⁴⁶ (arrow), which is replaced functionally in LpMip with a neighbouring phenylalanine residue. (C) The NMR structure of BpML1 confirms the crystallographic data and identifies flexibility within the active site. Left: cartoon of the NMR structure of BpML1 bound to ligand (yellow; PDB code 2K07) shows a very similar architecture to the crystal structure (A). Right: the comparison of bound (yellow) and apo protein (pink; PDB code 2KE0) shows significant conformational flexibility in the ligand-binding β 3a strand (arrow) and the β 4– β 5 loop (arrowhead). Both structures shown are representative for an ensemble of 20 structures consistent with the data.

(Figure 2A). Intriguingly, although BpML1 is a very active PPIase (I.H. Norville, N.J. Harmer, S. Harding, G. Fischer, K. Keith, K. Brown, M. Sarkar-Tyson and R.W. Titball, unpublished work), the conformation of the peptide is inconsistent with the expected binding for a proline-containing peptide. The proline side chain does not sit in the deep pocket of the enzyme: complexes with the inhibitor FK506 (see Supplementary Figure S1B [38]) and with a *cis*-peptide [35] have defined this as the likely site for *cis*–*trans* isomerization. In contrast, this site is occupied by a valine side chain (Figure 2B). Furthermore, the overall conformation of the peptide is highly diverged from the expected peptide orientation, suggested by structures of rapamycin or peptide-bound FKBP (Figure 2C [34,35,38]). We conclude that, although BpML1 is a *bona fide* PPIase, this peptide binding is not representative of the binding of substrates for pre-prolyl-peptide *cis*–*trans* isomerization.

However, the peptide binding is strikingly similar to the structure of hFKBP12 (human FKBP12) in complex with the TGF β RI (transforming growth factor β receptor I), bone morphogenetic protein receptor 1B and the activin type I receptor (PDB code 3H9R) [39] (Figure 2D; see Supplementary Figure S3 available at <http://www.BiochemJ.org/bj/437/bj4370413add.htm>). Eukaryotic FKBP forms physiologically important complexes with other proteins, binding partner proteins to modulate their activity [40,41], in addition to their roles in protein folding. In particular, the BpML1 peptide forms a short helix, in a similar conformation to the receptor helices that binds to hFKBP12; and each of these receptors places a leucine side chain into the deep pocket of

hFKBP12, reminiscent of the valine residue observed in BpML1. These observations suggest that, like hFKBP12, BpML1 is likely to form complexes with other proteins in the cell in addition to its role as a PPIase. hFKBP12 masks a multiple phosphorylation peptide (the Gly-Ser region) in TGF β RI, and locks the receptor into an inactive conformation to ensure that there is no activation in the absence of an extracellular signal [41]. As bacteria require robust signalling networks to respond appropriately to their surroundings, similar roles in dampening signalling noise are conceivable for BpML1.

X-ray and NMR structures of BPSS1823 reveal intrinsic flexibility in key active-site residues

The X-ray structure presented here diffracted to 0.91 Å. This resolution is high enough to reveal details of structural flexibility that cannot be observed at lower resolution. At this resolution, we can observe that 18% of the amino acid side chains (not including alanine and glycine residues) display multiple conformations. The majority of these residues are distant from the active site, in largely solvent exposed parts of the molecule. In addition to these amino acids, four alternative conformations are observed in the active site. First, the pair of Leu⁻⁶ from the binding peptide and Ile⁹³ displays correlated alternative conformers (see Supplementary Figure S4 available at <http://www.BiochemJ.org/bj/437/bj4370413add.htm>). More importantly, both Asp⁴⁴ and Tyr⁸⁹ show significant flexibility,

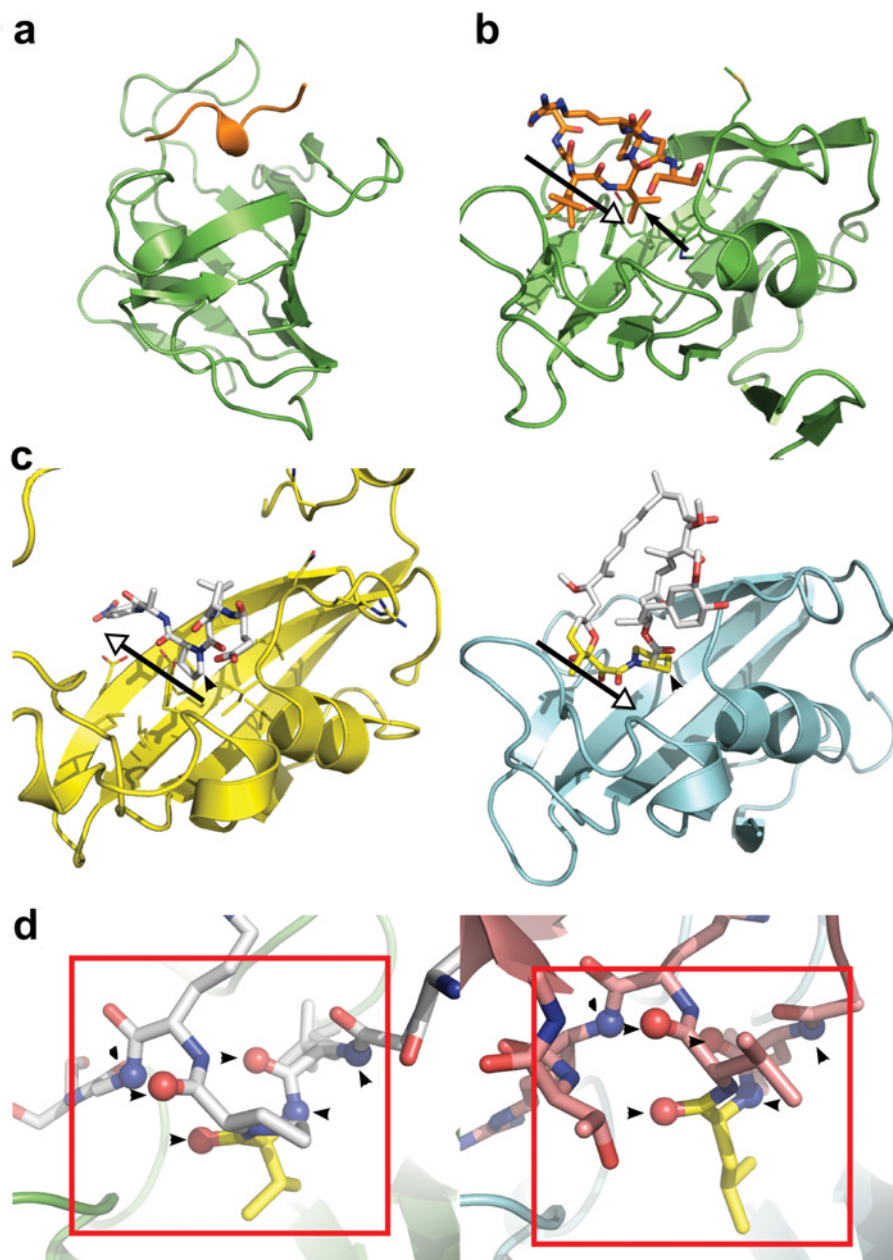


Figure 2 BpML1 binding to thrombin recognition peptide suggests that the protein is involved in protein–protein interactions

(a) Analysis of crystal packing in the X-ray structure of BpML1 (PDB code 2Y78) shows a helical peptide binding to the active site. Cartoon is shown of BpML1 (green) and the peptide derived from cloning (orange). (b) The peptide binds with a valine side chain (black arrow) in the heart of the enzyme active site. The peptide is represented by orange sticks, with BpML1 as a green cartoon. The black open-headed arrow indicates the direction of the peptide, N- to C-terminus. (c) The peptide binding is unlikely to represent a substrate for the PPlase activity. Comparison with the structure of a *cis*-prolyl-peptide bound to SlyD from *T. thermophilus* (left, yellow; PDB code 3LU0) and FK-506 bound to hFKBP12 (right, cyan; FK-506 pseudopeptide shown in yellow; PDB code 1FKJ) shows that a *bona fide cis*-proline peptide lying in the opposite orientation (black open-headed arrows); and that a prolyl or pseudoprolyl side chain occupies the active site (black arrowheads). (d) BpML1 peptide binding mimics hFKBP12 binding to TGF β R1. Left: BpML1 (green) binding to peptide (white sticks). Right: hFKBP12 (cyan) binding to a helix from TGF β R1 (pink sticks). The side chains binding to the heart of the active sites are coloured yellow. Note the similarity of the positions of the carbonyls in the red boxes. Six peptide main chain atoms making direct or through single water-mediated hydrogen bonds with BpML1 are shown as spheres on top of the sticks, and are further indicated by black arrowheads.

with hydrogen-bond donor and acceptor atoms moving by up to 1.5 Å between the observed extremes (Figure 3). The refined positions probably represent maxima within the electron density: the two residues therefore probably sample a larger range of positions. Similar flexibility is not observed in the 0.92 Å structure of unliganded hFKBP12 (see Supplementary Figure S5 available at <http://www.BiochemJ.org/bj/437/bj4370413add.htm> [42]), indicating that this is not an artefact of the software used.

These two amino acids provide the only sources of hydrogen-bond donors and acceptors in the BpML1 active site; and mutations of these residues in LpMip significantly reduce the activity of the enzyme [43]. As many proposed mechanisms of action of the enzyme involve these amino acids, this unexpected flexibility is highly suggestive of a role in catalysis. Accordingly, we examined the NMR structures of free and inhibitor-bound BpML1 to examine whether these also are consistent with a

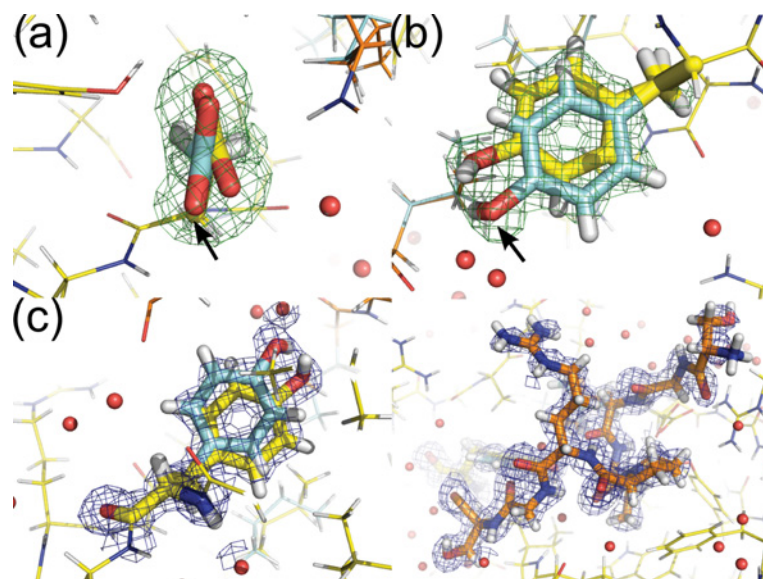


Figure 3 The ultra-high-resolution X-ray structure of BpML1 (PDB code 2Y78) shows multiple conformers of key ligand-binding residues

(a) Asp⁴⁴, which accepts a key hydrogen bond from the bound peptide backbone, shows two conformers for the side chain. The distance between the two conformations for O_{δ2} is 0.9 Å. The higher-occupancy conformation makes an additional hydrogen bond to the bound peptide backbone, while the other makes two additional hydrogen bonds to other residues of BpML1. (b) Tyr⁸⁹, the only hydrogen-bond donor in the active-site pocket, also shows a range of conformations. The distance between the O_γ atoms is 1.5 Å. One conformation is consistent with a direct (3.0 Å) hydrogen bond to the peptide, while the other makes a water-mediated hydrogen bond to the peptide. Lower-occupancy forms are indicated by a black arrow. (c) Representative electron density for a multiple conformer residue (Tyr⁸⁹, left) and the peptide binding to the active site (right). Colours: BpML1, yellow; binding peptide, orange; multiple conformation at lower occupancy, cyan; mF_o - DF_c simulated annealing omit map (side chains truncated to C_β) contoured at 3σ, green. 2mF_o - DF_c map for the final structure contoured at 1σ, blue.

pronounced flexibility for Asp⁴⁴ and Tyr⁸⁹. Strikingly, the side chain of Asp⁴⁴ shows a wide range of conformations (see Supplementary Figure S6 available at <http://www.BiochemJ.org/bj/437/bj4370413add.htm>). This is quite unusual for a residue that is apparently making a hydrogen-bond interaction with the bound ligand. In contrast, the side chain of Tyr⁸⁹ adopts two preferred rotamers, showing a classical alternative conformation. This contrasts with other well-conserved ligand-interacting residues (e.g. Trp⁶⁶), which show only a single conformation across 20 models, consistent with the data.

This unusual flexibility of these highly conserved side chains in the active site strongly suggests a role for this flexibility in function. The side chains make hydrogen-bonding interactions in at least one of their conformers, indicating that they do not lack a stable conformation. The conformations observed in the structures offer a tantalizing possible role in catalysis: superimposition of the extended prolyl-peptide from the recently solved FKBP-peptide structure [35] shows that one of the Tyr⁸⁹ conformers would be perfectly placed to stabilize the peptide nitrogen in an intermediate state between the *cis* and *trans* peptide. One alternative conformation of Asp⁴⁴ could interact with and stabilize the peptide backbone of the substrate. These observations suggest that Tyr⁸⁹ and Asp⁴⁴ are natively flexible in BpML1, and that this flexibility is likely to be relevant to catalysis.

The structure of BpML1 bound to cycloheximide *N*-ethylethanoate reveals a novel mode of inhibitor binding

We previously showed that BpML1 binds to rapamycin, which inhibits all known FKBP (I.H. Norville, N.J. Harmer, S. Harding, G. Fischer, K. Keith, K. Brown, M. Sarkar-Tyson and R.W. Titball, unpublished work). Cycloheximide, an inhibitor of eukaryotic protein synthesis, is an unrelated compound that has previously been shown to inhibit the PPIase activity of both hFKBP12 and

LpMip (Figure 4A) [44]. Cycloheximide *N*-ethylethanoate, which is also active against hFKBP12, inhibited the PPIase activity of BpML1 (Figure 4B): the observed K_1 of $6.5 \pm 1.0 \mu\text{M}$ is similar to the K_1 reported for this compound towards FKBP12 ($4.4 \mu\text{M}$). As there is no extant structure of cycloheximide *N*-ethylethanoate with an FKBP, we determined the structure of BpML1 bound to cycloheximide *N*-ethylethanoate by NMR. This structure reveals that the compound binds to the active site (Figure 4C). However, although the compound binds to most of the highly conserved side chains, the major interactions occur with the $\beta 3b$ - $\alpha 1$ and $\beta 4$ - $\beta 5$ loops (Figure 4D). In fact, hydrophobic contacts are formed with residues Ala⁹⁴ and Ile⁹⁸, outside the core active site. No significant interactions take place with the other sides of the catalytic bowl of the FKBP, with the highly conserved active-site residues Tyr³³ and Phe⁵⁷ in particular having no contact with the inhibitor. In comparison, previously observed inhibitors such as FK506, rapamycin and other synthetic inhibitors [38,45,46] tend to bind more broadly across the catalytic bowl, and contact conserved active-site residues across it (Figure 5). Many of these inhibitors also make extensive contacts with the same two loops as cycloheximide *N*-ethylethanoate.

Remarkably, the conformation of cycloheximide *N*-ethylethanoate mimics that of the peptide found in the BpML1 crystal structure, and the structure of hFKBP12 bound to TGF β RI (Figure 4E). Thus cycloheximide *N*-ethylethanoate represents a new class of FKBP inhibitors, mimicking the binding of FKBP to proteins to modulate activity, rather than proline-peptides as rapamycin and FK506 do.

Conclusions

In the present paper, we report the structure of BpML1, a Mip homologue of *B. pseudomallei*, which was determined by X-ray crystallography and NMR in parallel. We show that

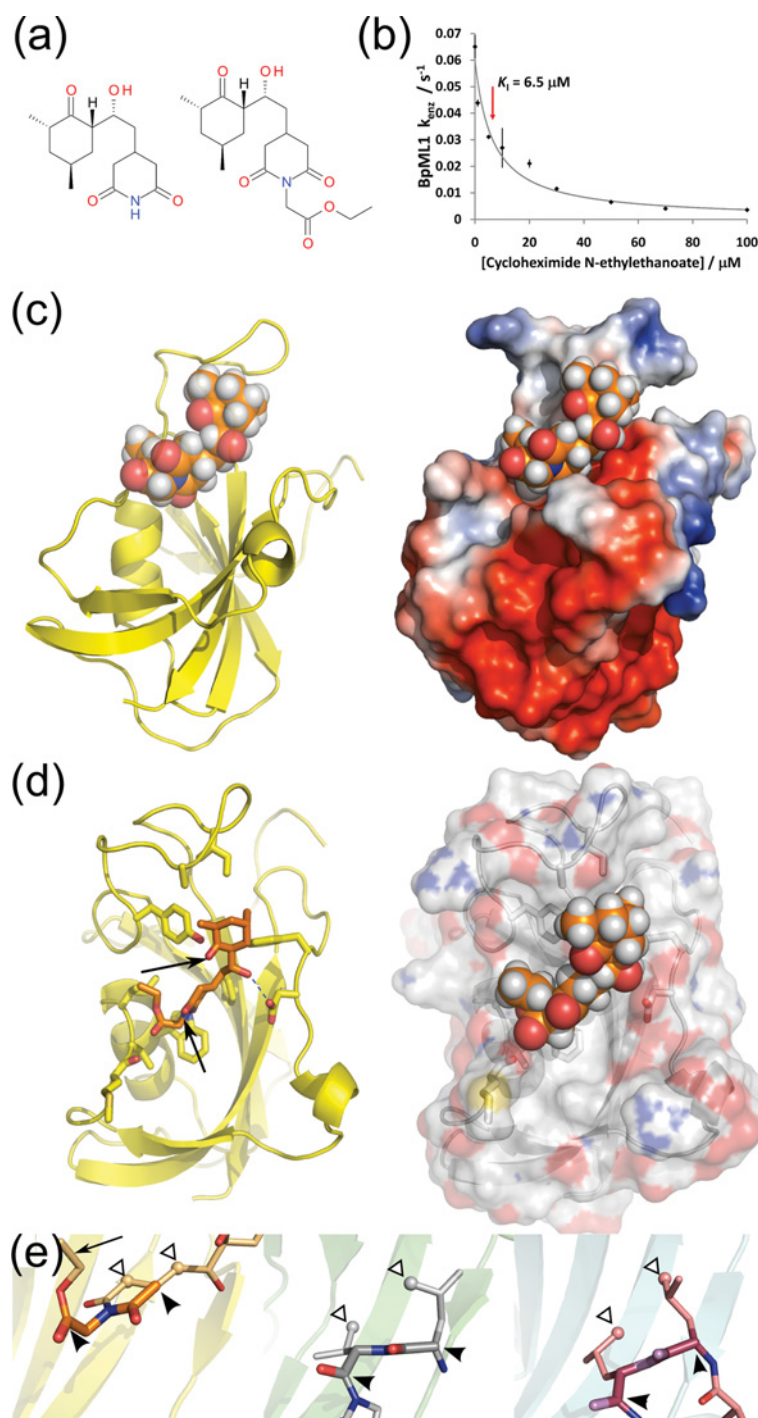


Figure 4 Cycloheximide *N*-ethylethanoate identifies a novel binding mode for FKBP inhibitors

(a) Structures of cycloheximide (left) and its derivative cycloheximide *N*-ethylethanoate (right). (b) Inhibition of BpML1 by cycloheximide *N*-ethylethanoate: cycloheximide *N*-ethylethanoate inhibited the PPlase activity of BpML1 in a dose-dependent manner, showing a K_I of $6.5 \pm 1.0 \mu\text{M}$. All experiments were performed in triplicate, and S.E.M. are shown. The continuous line shows the inhibition curve for fitted values of the inhibition parameters. (c) Overview of the NMR structure of cycloheximide *N*-ethylethanoate (orange spheres) bound to BpML1 (PDB code 2K07). Left: BpML1 shown as a yellow cartoon. Right: surface of BpML1 shown, coloured by charge density (red: negative; blue: positive). Charge density was calculated using APBS [49] and PDB2PQR [50]. (d) Close-up view of active-site residues binding to cycloheximide *N*-ethylethanoate. Residues within 3.5 Å of cycloheximide *N*-ethylethanoate are shown as sticks. Left: BpML1 shown as a cartoon, cycloheximide *N*-ethylethanoate shown as sticks. The hydrogen bond between the Cycloheximide *N*-ethylethanoate hydroxyl and Asp⁴⁴ is especially noteworthy; and that some functional groups of cycloheximide *N*-ethylethanoate (arrowed) do not make any interactions with the protein, and could be altered. Right: BpML1 is shown as semi-transparent surface, cycloheximide *N*-ethylethanoate as spheres. Cycloheximide *N*-ethylethanoate shows good shape complementarity to BpML1, consistent with its micromolar inhibitory activity. (e) Cycloheximide *N*-ethylethanoate mimics the binding of peptides to FKBP. Left: cycloheximide *N*-ethylethanoate (light-orange sticks; atoms mimicking the peptide coloured bolder and shown thicker) bound to BpMip (yellow cartoon; PDB code 2K07). Centre: peptide (white sticks; atoms equivalent to those highlighted left shown light grey and thicker) bound to BpMip (green cartoon; PDB code 2Y78). Right: helix from TGFβRI (pink sticks) binding to hFKBP12 (cyan cartoon; PDB code 1B6C). The relevant portions of each peptide are highlighted with black arrowheads, while hydrophobic side chains/cycloheximide *N*-ethylethanoate atoms binding to the protein are highlighted with white arrowheads. The black arrow indicates a section of cycloheximide *N*-ethylethanoate that binds to a BpML1 pocket that is not accessed by the peptides. Note how the cycloheximide *N*-ethylethanoate molecule binds closer to the β4–β5 loop than the peptides.

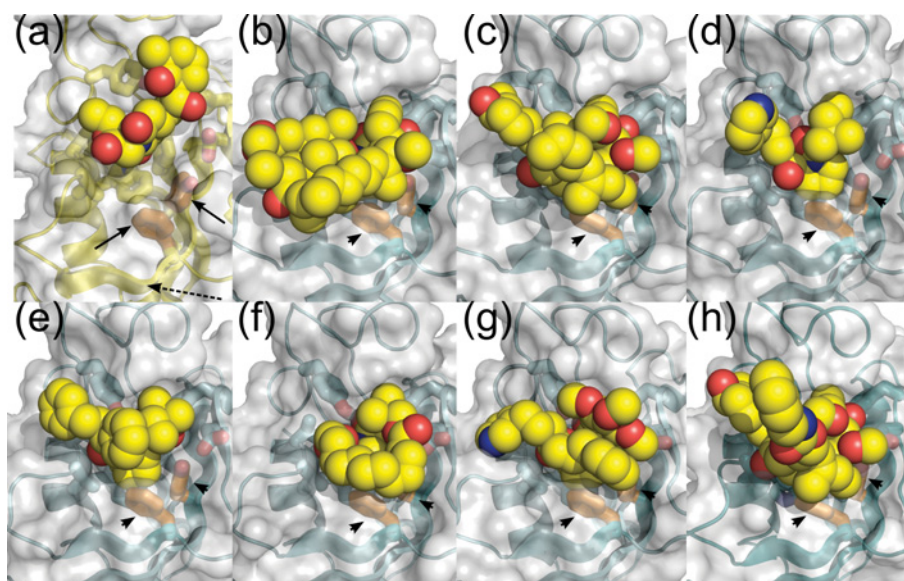


Figure 5 Comparison of the binding of FKBP inhibitors to FKBP indicates that cycloheximide *N*-ethylethanoate represents a novel class of inhibitor

Inhibitors are shown as all heavy atom spherical models, with carbon coloured yellow, oxygen coloured red and nitrogen coloured blue; proteins are shown as white semi-transparent surfaces, with cartoon beneath. Cartoon colours: BpMip, yellow; FKBP12, cyan. The nine most conserved active-site residues of FKBP are shown as sticks, with carbon coloured as for the main chain, and other atoms as above. Side chains Tyr³³ and Phe⁵⁷ of BpMip do not contact the inhibitor, and are highlighted with carbon coloured orange and with black arrowheads. (a) BpMip binding to cycloheximide *N*-ethylethanoate (the present study; PDB code 2K07). (b) FKBP12 binding to rapamycin (PDB code 2DG3). (c) FKBP12 binding to FK-506 (PDB code 1FKJ). (d) FKBP12 binding to the neurotrophic ligand GPI-1046 (PDB code 1F40). (e–g) FKBP12 binding to synthetic high-affinity ligands (PDB codes: 1FKG, 1FKI, 1J4R). (h) FKBP12 binding to a synthetic dimeric ligand (PDB code 1A7X). Note that cycloheximide *N*-ethylethanoate occupies a distinct area of the protein, and in particular does not interact with the β 3b strand (black broken arrow in a).

this enzyme is competent in binding to peptides or the class inhibitor cycloheximide *N*-ethylethanoate. Intriguingly, we show that the peptide bound in the structure is not a *cis*-proline, but a small helical peptide that mimics TGF β R bound to hFKBP12; and that cycloheximide *N*-ethylethanoate binds in the active site in a way that mimics this peptide, rather than the catalytic peptides that are mimicked by other class inhibitors. These results suggest that Mips (and potentially other bacterial FKBP), like their eukaryotic cousins, are competent to bind peptides in a helical conformation. This suggests that BpML1 and other Mips have roles in protein–protein interactions, perhaps as modulators of signalling, in addition to their chaperone functions. Consistent with this observation, deletion of BpML1 abolished *B. pseudomallei* showing a pleiotrophic phenotype, including loss of motility which might suggest a role in the control of the flagellar motors (I. Norville, N. Harmer, S. Harding, G. Fischer, K. Keith, K. Brown, M. Sarkar-Tyson and R. Titball, unpublished work).

The ultra-high-resolution crystal structure of BpML1 revealed that two highly conserved active-site side chains, Asp⁴⁴ and Tyr⁸⁹, show unusual flexibility. These observations were confirmed by NMR, and suggest that these side chains require flexibility, even in a ligand-bound form, for performing their roles in catalysis. However, it is not clear as to whether this represents a general mechanism for FKBP or a specific case of BpML1: this enzyme is up to 6-fold more active than previously described FKBP, and so the flexibility that we observed may be an adaptation of this enzyme to provide it with a greater rate enhancement.

The structure of the cycloheximide *N*-ethylethanoate complex with BpML1 suggests that this compound might provide an excellent starting point for novel drug development. The binding site for cycloheximide *N*-ethylethanoate, uniquely for FKBP

inhibitors of known structure, is focused on the β 3b– α 1 and β 4– β 5 loops, and contacts residues outside the active site in the β 4– β 5 loop. This new interaction offers a greater possibility of obtaining a selective compound that would not inhibit human proteins: the β 4– β 5 loop, in particular, shows much greater diversity between species than the active site. Furthermore, we show in the present study that both of these loops show considerable flexibility, increasing the likelihood of a species-specific-induced fit.

We conclude that the bacterial FKBP are likely to be a more diverse and functionally rich protein family than has previously been appreciated. In consequence of this, their validated role in the pathogenesis of several micro-organisms, and the availability of multiple inhibitors for this protein class, they show great promise for antimicrobial drug discovery.

AUTHOR CONTRIBUTION

Isobel Norville, Katherine O'Shea and Suxin Zheng designed and performed experiments; Mitali Sarkar-Tyson and Richard Titball, together with Gabriele Varani and Nicholas Harmer conceived and designed the study, and edited the paper before submission. Gabriele Varani and Nicholas Harmer supervised the project and wrote the paper.

ACKNOWLEDGEMENTS

N.H. acknowledges the Diamond Synchrotron (Oxford, U.K.) for X-ray data collection. G.V. acknowledges the protein expression team at the SSGCID (Seattle Structural Genomics Center for Infectious Disease), and access to facilities at Pacific Northwest National Laboratory (Richland, WA, U.S.A.) for NMR data collection.

FUNDING

This work was supported by the University of Exeter (to K.O.S. and N.H.); the UK Ministry of Defence (to I.N. and M.S.-T.); and the National Institutes of Health Institute of Allergy and Infectious Disease [Federal Contract HHSN27200700057C (to S.Z. and G.V.)]

REFERENCES

- Wiersinga, W. J., van der Poll, T., White, N. J., Day, N. P. and Peacock, S. J. (2006) Melioidosis: insights into the pathogenicity of *Burkholderia pseudomallei*. *Nat. Rev. Microbiol.* **4**, 272–282
- White, N. (2003) Melioidosis. *Lancet* **361**, 1715–1722
- Cheng, A. C. and Currie, B. J. (2005) Melioidosis: epidemiology, pathophysiology, and management. *Clin. Microbiol. Rev.* **18**, 383–416
- Rotz, L. D., Khan, A. S., Lillibridge, S. R., Ostroff, S. M. and Hughes, J. M. (2002) Public health assessment of potential biological terror agents. *Emerg. Infect. Dis.* **8**, 225–230
- Kang, C. B., Hong, Y., Dhe-Paganon, S. and Yoon, H. S. (2008) FKBP family proteins: immunophilins with versatile biological functions. *Neurosignals* **16**, 318–325
- Cianciotto, N. P., Eisenstein, B. I., Mody, C. H., Toews, G. B. and Engleberg, N. C. (1989) A *Legionella pneumophila* gene encoding a species-specific surface protein potentiates initiation of intracellular infection. *Infect. Immun.* **57**, 1255–1262
- Lundemose, A. G., Kay, J. E. and Pearce, J. H. (1993) *Chlamydia trachomatis* Mip-like protein has peptidyl-prolyl *cis/trans* isomerase activity that is inhibited by FK506 and rapamycin and is implicated in initiation of chlamydial infection. *Mol. Microbiol.* **7**, 777–783
- Leuzzi, R., Serino, L., Scarselli, M., Savino, S., Fontana, M. R., Monaci, E., Taddei, A., Fischer, G., Rappuoli, R. and Pizza, M. (2005) Ng-MIP, a surface-exposed lipoprotein of *Neisseria gonorrhoeae*, has a peptidyl-prolyl *cis/trans* isomerase (PPIase) activity and is involved in persistence in macrophages. *Mol. Microbiol.* **58**, 669–681
- Moro, A., Ruiz-Cabello, F., Fernandez-Cano, A., Stock, R. P. and Gonzalez, A. (1995) Secretion by *Trypanosoma cruzi* of a peptidyl-prolyl *cis-trans* isomerase involved in cell infection. *EMBO J.* **14**, 2483–2490
- Helbig, J. H., Konig, B., Knosp, H., Bubert, B., Yu, C., Luck, C. P., Riboldi-Tunnicliffe, A., Hilgenfeld, R., Jacobs, E., Hacker, J. and Fischer, G. (2003) The PPIase active site of *Legionella pneumophila* Mip protein is involved in the infection of eukaryotic host cells. *Biol. Chem.* **384**, 125–137
- Wagner, C., Khan, A. S., Kamphausen, T., Schmausser, B., Unal, C., Lorenz, U., Fischer, G., Hacker, J. and Steinert, M. (2007) Collagen binding protein Mip enables *Legionella pneumophila* to transmigrate through a barrier of NCI-H292 lung epithelial cells and extracellular matrix. *Cell. Microbiol.* **9**, 450–462
- Zang, N., Tang, D. J., Wei, M. L., He, Y. Q., Chen, B., Feng, J. X., Xu, J., Gan, Y. Q., Jiang, B. L. and Tang, J. L. (2007) Requirement of a mip-like gene for virulence in the phytopathogenic bacterium *Xanthomonas campestris* pv. *campestris*. *Mol. Plant Microbe Interact.* **20**, 21–30
- Studier, F. W. (2005) Protein production by auto-induction in high-density shaking cultures. *Protein Expression Purif.* **41**, 207–234
- Leslie, A. G. W. (1992) Recent changes to the MOSFLM package for processing film and image plate data. Joint CCP4 and ESF-EAMCB Newsletter on Protein Crystallography, No. 26
- Evans, P. R. (2005) Scaling and assessment of data quality. *Acta Crystallogr. Sect. D Biol. Crystallogr.* **62**, 72–82
- Stein, N. (2008) CHAINSAW: a program for mutating pdb files used as templates in molecular replacement. *J. Appl. Crystallogr.* **41**, 641–643
- McCoy, A. J., Grosse-Kunstleve, R. W., Adams, P. D., Winn, M. D., Storoni, L. C. and Read, R. J. (2007) Phaser crystallographic software. *J. Appl. Crystallogr.* **40**, 658–674
- Emsley, P., Lohkamp, B., Scott, W. G. and Cowtan, K. (2010) Features and development of Coot. *Acta Crystallogr. Sect. D Biol. Crystallogr.* **66**, 486–501
- Adams, P. D., Grosse-Kunstleve, R. W., Hung, L.-W., Ioerger, T. R., McCoy, A. J., Moriarty, N. W., Read, R. J., Sacchettini, J. C., Sauter, N. K. and Terwilliger, T. C. (2002) PHENIX: building new software for automated crystallographic structure determination. *Acta Crystallogr. Sect. D Biol. Crystallogr.* **58**, 1948–1954
- Davis, I. W., Leaver-Fay, A., Chen, V. B., Block, J. N., Kapral, G. J., Wang, X., Murray, L. W., Arendall, III, B., Snoeyink, J., Richardson, J. S. and Richardson, D. C. (2007) MOLPROBITY: all-atom contacts and structure validation for proteins and nucleic acids. *Nucleic Acids Res.* **35**, W375–W383
- Kay, L. E., Xu, G. Y., Singer, A. U., Muhandiram, D. R. and Formankay, J. D. (1993) A gradient-enhanced HCCH TOCSY experiment for recording side-chain H-1 and C-13 correlations in H₂O samples of proteins. *J. Magn. Reson. B* **101**, 333–337
- Muhandiram, D. R., Xu, G. Y. and Kay, L. E. (1993) An enhanced-sensitivity pure absorption gradient 4d N-15, C-13-edited NOESY experiment. *J. Biomol. NMR* **3**, 463–470
- Yamazaki, T., Lee, W., Revington, M., Mattiello, D. L., Dahlquist, F. W., Arrowsmith, C. H. and Kay, L. E. (1994) An HNCA pulse scheme for the backbone assignment of N-15, C-13, H-2-labeled proteins-application to a 37-kDa Trp repressor DNA complex. *J. Am. Chem. Soc.* **116**, 6464–6465
- Muhandiram, D. R. and Kay, L. E. (1994) Gradient-enhanced triple-resonance 3-dimensional NMR experiments with improved sensitivity. *J. Magn. Reson. B* **103**, 203–216
- Peterson, R. D., Theimer, C. A., Wu, H. H. and Feigon, J. (2004) New applications of 2D filtered/edited NOESY for assignment and structure elucidation of RNA and RNA-protein complexes. *J. Biomol. NMR* **28**, 59–67
- Zwahlen, C., Legault, P., Vincent, S. J. F., Greenblatt, J., Konrat, R. and Kay, L. E. (1997) Methods for measurement of intermolecular NOEs by multinuclear NMR spectroscopy: application to a bacteriophage lambda N-peptide/boxB RNA complex. *J. Am. Chem. Soc.* **119**, 6711–6721
- Delaglio, F., Grzesiek, S., Vuister, G. W., Zhu, G., Pfeifer, J. and Bax, A. (1995) NMRPipe: a multidimensional spectral processing system based on Unix pipes. *J. Biomol. NMR* **6**, 277–293
- Vranken, W. F., Boucher, W., Stevens, T. J., Fogh, R. H., Pajon, A., Llinas, P., Ulrich, E. L., Markley, J. L., Ionides, J. and Laue, E. D. (2005) The CCPN data model for NMR spectroscopy: development of a software pipeline. *Proteins* **59**, 687–696
- Güntert, P. (2003) Automated NMR protein structure calculation. *Prog. Nucl. Magn. Reson. Spectrosc.* **43**, 105–125
- Herrmann, T., Güntert, P. and Wüthrich, K. (2002) Protein NMR structure determination with automated NOE assignment using the new software CANDID and the torsion angle dynamics algorithm DYANA. *J. Mol. Biol.* **319**, 209–227
- Fischer, G., Bang, H. and Mech, C. (1984) Detection of enzyme catalysis for *cis-trans* isomerization of peptide-bonds using proline-containing peptides as substrates. *Biomed. Biochim. Acta* **43**, 1101–1111
- Kullertz, G., Luthe, S. and Fischer, G. (1998) Semiautomated microtiter plate assay for monitoring peptidyl-prolyl *cis/trans* isomerase activity in normal and pathological human sera. *Clin. Chem.* **44**, 502–508
- Williams, J. W. and Morrison, J. F. (1979) The kinetics of reversible tight-binding inhibition. *Methods Enzymol.* **63**, 437–467
- Ceymann, A., Horstmann, M., Ehses, P., Schweimer, K., Paschke, A. K., Steinert, M. and Faber, C. (2008) Solution structure of the *Legionella pneumophila* Mip-rapamycin complex. *BMC Struct. Biol.* **8**, 17
- Löw, C., Neumann, P., Tidow, H., Weininger, U., Haupt, C., Friedrich-Epler, B., Scholz, C., Stubbs, M. T. and Balbach, J. (2010) Crystal structure determination and functional characterization of the metallochaperone SlyD from *Thermus thermophilus*. *J. Mol. Biol.* **398**, 375–390
- Pereira, P. J., Vega, M. C., Gonzalez-Rey, E., Fernandez-Carazo, R., Macedo-Ribeiro, S., Gomis-Ruth, F. X., Gonzalez, A. and Coll, M. (2002) *Trypanosoma cruzi* macrophage infectivity potentiator has a rotamase core and a highly exposed α -helix. *EMBO Rep.* **3**, 88–94
- Riboldi-Tunnicliffe, A., Konig, B., Jessen, S., Weiss, M. S., Rahfeld, J., Hacker, J., Fischer, G. and Hilgenfeld, R. (2001) Crystal structure of Mip, a prolylisomerase from *Legionella pneumophila*. *Nat. Struct. Biol.* **8**, 779–783
- Wilson, K. P., Yamashita, M. M., Sintchak, M. D., Rotstein, S. H., Murcko, M. A., Boger, J., Thomson, J. A., Fitzgibbon, M. J., Black, J. R. and Navia, M. A. (1995) Comparative X-ray structures of the major binding protein for the immunosuppressant FK506 (tacrolimus) in unliganded form and in complex with FK506 and rapamycin. *Acta Crystallogr. Sect. D Biol. Crystallogr.* **51**, 511–521
- Huse, M., Chen, Y. G., Massague, J. and Kuriyan, J. (1999) Crystal structure of the cytoplasmic domain of the type I TGF β receptor in complex with FKBP12. *Cell* **96**, 425–436
- Chelu, M. G., Danila, C. I., Gilman, C. P. and Hamilton, S. L. (2004) Regulation of ryanodine receptors by FK506 binding proteins. *Trends Cardiovasc. Med.* **14**, 227–234
- Huse, M., Muir, T. W., Xu, L., Chen, Y. G., Kuriyan, J. and Massague, J. (2001) The TGF β receptor activation process: an inhibitor- to substrate-binding switch. *Mol. Cell* **8**, 671–682
- Szep, S., Park, S., Boder, E. T., Van Duyn, G. D. and Saven, J. G. (2009) Structural coupling between FKBP12 and buried water. *Proteins* **74**, 603–611
- Wintermeyer, E., Ludwig, B., Steinert, M., Schmidt, B., Fischer, G. and Hacker, J. (1995) Influence of site specifically altered Mip proteins on intracellular survival of *Legionella pneumophila* in eukaryotic cells. *Infect. Immun.* **63**, 4576–4583
- Christner, C., Wyrwa, R., Marsch, S., Kullertz, G., Thiericke, R., Grabley, S., Schumann, D. and Fischer, G. (1999) Synthesis and cytotoxic evaluation of cycloheximide derivatives as potential inhibitors of FKBP12 with neuroregenerative properties. *J. Med. Chem.* **42**, 3615–3622

- 45 Sich, C., Improta, S., Cowley, D. J., Guenet, C., Merly, J. P., Teufel, M. and Saudek, V. (2000) Solution structure of a neurotrophic ligand bound to FKBP12 and its effects on protein dynamics. *Eur. J. Biochem.* **267**, 5342–5355
- 46 Sun, F., Li, P., Ding, Y., Wang, L., Bartlam, M., Shu, C., Shen, B., Jiang, H., Li, S. and Rao, Z. (2003) Design and structure-based study of new potential FKBP12 inhibitors. *Biophys. J.* **85**, 3194–3201
- 47 Cornilescu, G., Delaglio, F. and Bax, A. (1999) Protein backbone angle restraints from searching a database for chemical shift and sequence homology. *J. Biomol. NMR* **13**, 289–302
- 48 Fulton, K. F., Jackson, S. E. and Buckle, A. M. (2003) Energetic and structural analysis of the role of tryptophan 59 in FKBP12. *Biochemistry* **42**, 2364–2372
- 49 Baker, N., Sept, D., Joseph, S., Holst, M. and McCammon, J. (2001) Electrostatics of nanosystems: application to microtubules and the ribosome. *Proc. Natl. Acad. Sci. U.S.A.* **98**, 10037–10041
- 50 Dolinsky, T. J., Czodrowski, P., Li, H., Nielsen, J. E., Jensen, J. H., Klebe, G. and Baker, N. A. (2007) PDB2PQR: expanding and upgrading automated preparation of biomolecular structures for molecular simulations. *Nucleic Acids Res.* **35**, W522–W525

Received 24 February 2011/13 May 2011; accepted 16 May 2011

Published as BJ Immediate Publication 16 May 2011, doi:10.1042/BJ20110345

SUPPLEMENTARY ONLINE DATA

The structure of a *Burkholderia pseudomallei* immunophilin–inhibitor complex reveals new approaches to antimicrobial development

Isobel H. NORVILLE*†, Katherine O'SHEA*†, Mitali SARKAR-TYSON†, Suxin ZHENG‡, Richard W. TITBALL*, Gabriele VARANI‡¹ and Nicholas J. HARMER*¹

*School of Biosciences, University of Exeter, Geoffrey Pope Building, Stocker Road, Exeter EX4 4QD, U.K., †Defence Science and Technology Laboratory, Porton Down, Salisbury, Wiltshire SP4 0JQ, U.K., and ‡Departments of Chemistry and Biochemistry, University of Washington, Box 351700, Seattle, WA 98195-1700, U.S.A.

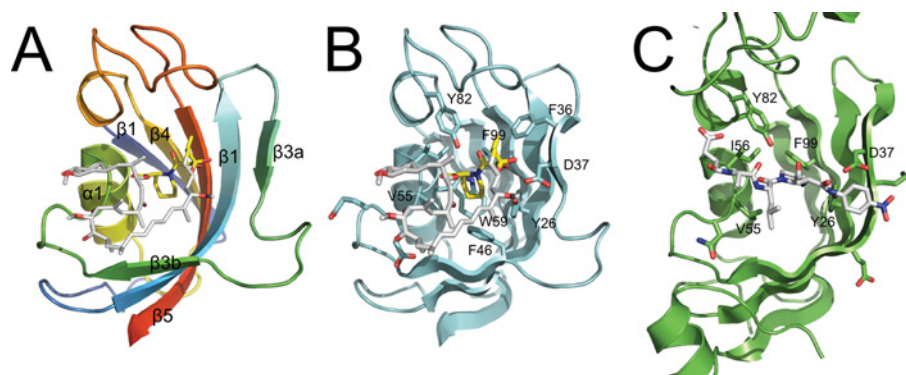


Figure S1 Structure and active site of FKBP

(A) The binding site for rapamycin defines the active site of FKBP. Shown is h-FKBP12 (rainbow cartoon: N-terminus, blue; C-terminus, red) bound to rapamycin (white/yellow sticks; PDB code 2DG3 [1]). The pseudo-proline-leucine dipeptide of rapamycin is shown with carbons coloured yellow, to highlight the proposed site of activity. (B) Rapamycin contacts closely a range of residues thought to be important in catalysis. All side chains within 4 Å of rapamycin are shown as sticks. Those side chains widely thought to be involved in catalysis are labelled. (C) An FKBP–peptide complex confirms the active site. Shown is the structure of *Thermus thermophilus* SlyD in complex with a peptide containing a *cis*-proline (PDB code 3LUO [2]). Protein is shown as a green cartoon, with side chains within 4 Å of the peptide shown as sticks. Peptide is shown as white sticks. The proposed active-site residues conserved in SlyD are indicated (using hFKBP12 numbering).

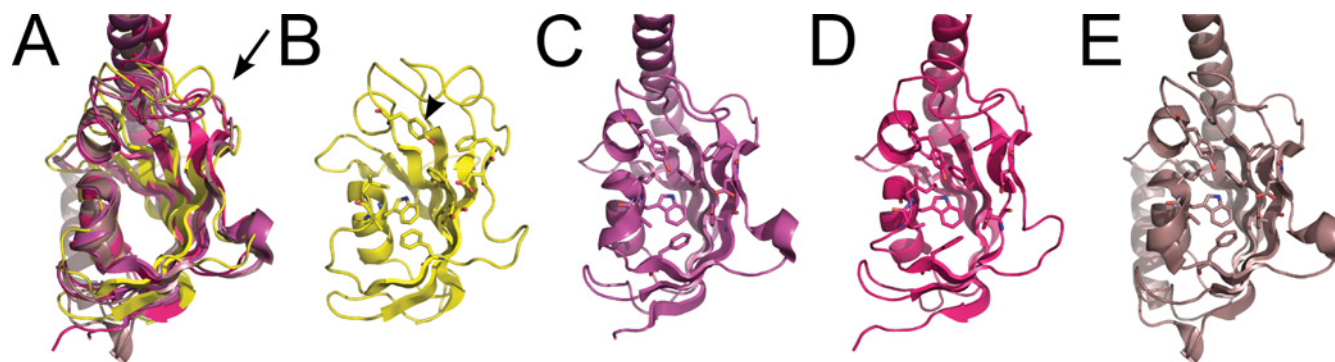


Figure S2 The active site of BpMip shows a significant distortion in comparison with other Mips

(A) Cartoon overlay of Mips from *B. pseudomallei* (yellow; PDB code 2KE0), *L. pneumophila* (apo form; magenta; PDB code 1FD9; rapamycin-bound; pink; PDB code 2VPN) and *T. cruzi* (chocolate; PDB code 1JVV). Note the BpMip β 4– β 5 loop (black arrow), which forms a very different conformation to that of other Mips. (B–E) Cartoons of Mips from *B. pseudomallei*, *L. pneumophila* (apo and rapamycin-bound) and *T. cruzi* respectively, with the eight best-conserved active-site residues shown as sticks. Coloured as above. Note the unusual location and conformation of Tyr⁸⁹ in BpMip (black arrowhead).

¹ Correspondence may be addressed to either of these authors (email varani@chem.washington.edu or N.J.Harmer@exeter.ac.uk).

The structural co-ordinates reported for *Burkholderia pseudomallei* peptidylprolyl *cis*–*trans* isomerase, *B. pseudomallei* peptidylprolyl *cis*–*trans* isomerase in complex with cycloheximide *N*-ethylethanoate and BPSS1823, a *B. pseudomallei* Mip-like chaperone, have been deposited in the PDB under codes 2KE0, 2K07 and 2Y78 respectively.

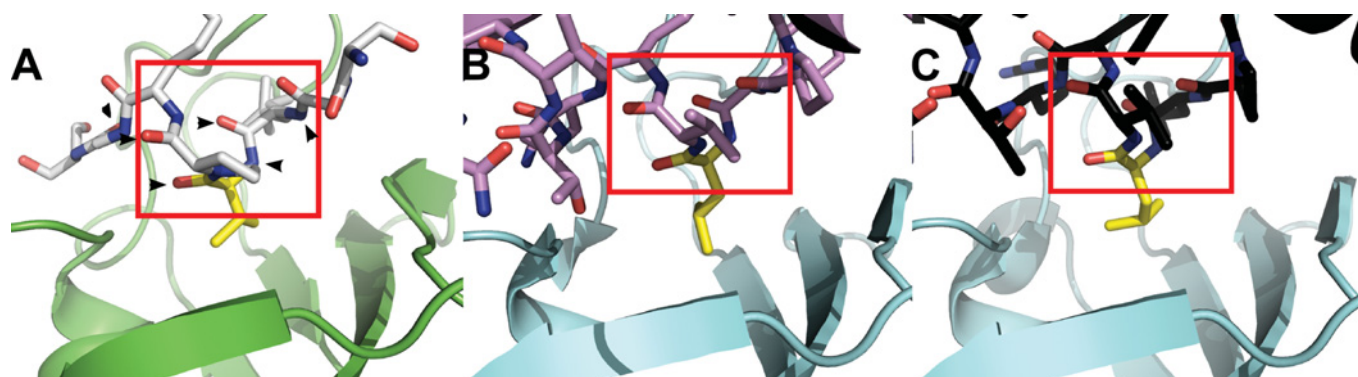


Figure S3 BpMip peptide binding mimics hFBKP12 binding to activin receptor (AR) and bone morphogenetic protein receptor type 1B (BMPRI1B)

(A) BpMip (green) binding to peptide (white sticks; PDB code 2Y78). (B) hFBKP12 (cyan) binding to a helix from activin receptor (violet sticks; PDB code 3H9R). (C) hFBKP12 (cyan) binding to a helix from BMPRI1B (black sticks; PDB code 3MDY). The side chains binding to the heart of the active sites are coloured yellow. Note the similarity of the positions of the carbonyls in the red boxes. Six peptide main chain atoms making direct or through single water hydrogen bonds with BpMip are indicated by black arrowheads.

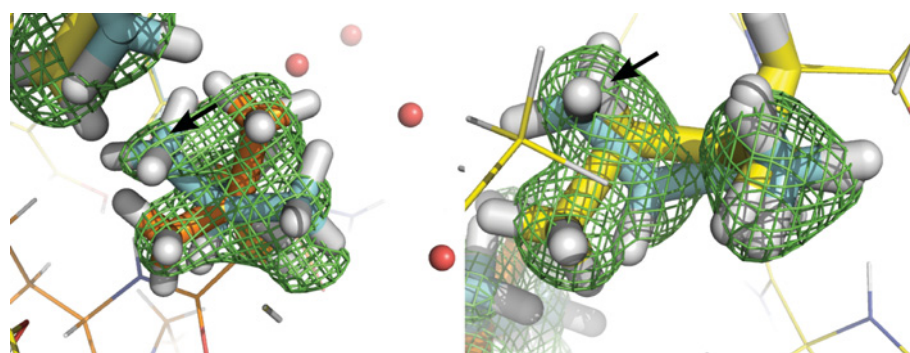


Figure S4 The ultra-high-resolution X-ray structure of BpMip (PDB code 2Y78) shows multiple conformers of ligand-binding residues

The hydrophobic residues Leu⁻⁶ (left) and Ile⁹⁸ (right) show coupled alternate conformers. The lower-occupancy conformer (black arrows) shows Leu⁻⁶ in a conformation closer to the protein, with Ile⁹⁸ moving away to accommodate this. Colours: BpMip, yellow; binding peptide, orange; multiple conformation at lower occupancy, cyan; $mF_o - DF_c$ simulated annealing omit map (side chains truncated to C_β) contoured at 3σ , green.

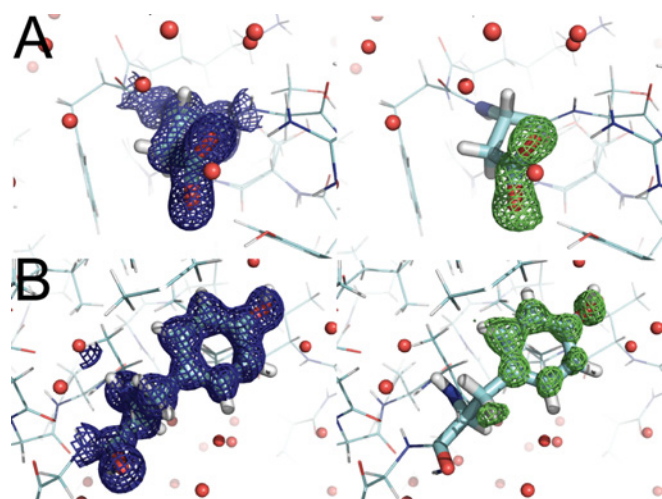


Figure S5 Alternative conformations of key active-site residues are not seen in human FKBP12 ultra-high-resolution structures

The co-ordinates and structure factors for the highest-resolution structure of human FKBP12 (PDB code 2PPN; resolution of 0.92 Å [3]) were re-refined using PHENIX, and the parameters used for the solution of the structure shown in the present study. Simulated annealing omit maps and the final refined density for Asp³⁷ and Tyr⁸² fail to show any evidence of alternative conformations. **(A)** Density for Asp³⁷; left, final refined density; right, omit map. **(B)** Density for Tyr⁸²; left, final refined density; right, omit map. Protein shown as cyan sticks, with relevant side chains shown as bolder sticks; $mF_o - DF_c$ simulated annealing omit map contoured at 3σ coloured green, and $2mF_o - DF_c$ map for the final structure contoured at 1σ , blue.

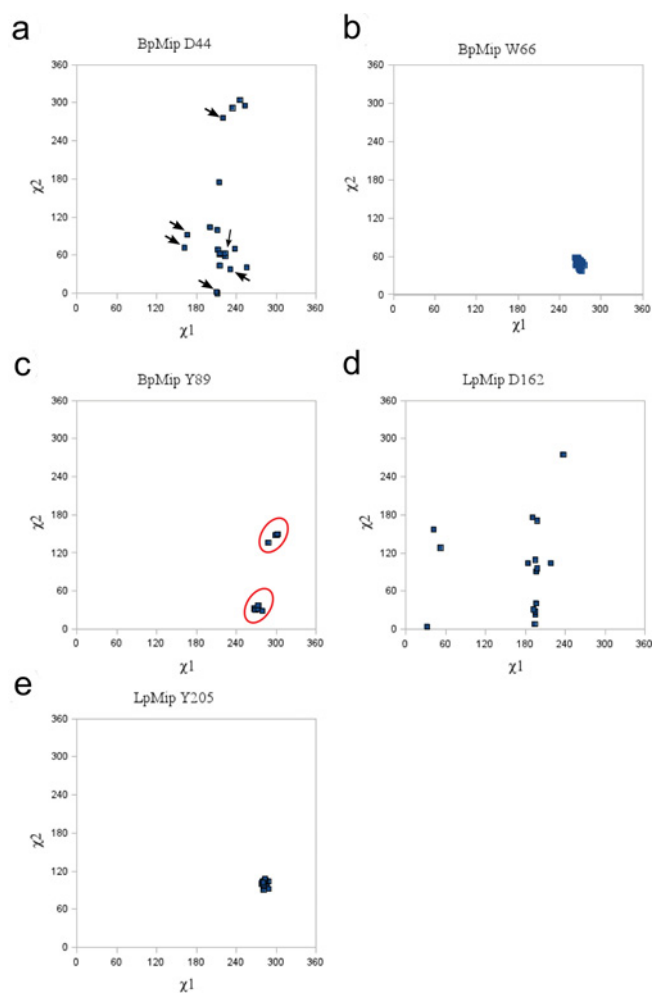


Figure S6 χ_1 – χ_2 plots for NMR structures of Mips indicate that Asp⁴⁴ and Tyr⁸⁹ have unusual flexibility in solution

χ_1 and χ_2 were calculated for Asp⁴⁴, Tyr⁸⁹ and Trp⁶⁶ (or LpMip equivalents) for all deposited models for BpMip bound to cycloheximide *N*-ethylethanoate (20 models; PDB code 2K07) and LpMip bound to rapamycin (16 models; PDB code 2VCD). **(a)** BpMip, Asp⁴⁴; **(b)** BpMip, Trp⁶⁶; **(c)** BpMip, Tyr⁸⁹; **(d)** LpMip, Asp¹⁶²; **(e)** LpMip, Tyr²⁰⁵. Asp⁴⁴ conformers that fail to make a hydrogen bond to cycloheximide *N*-ethylethanoate are indicated by arrows. Note the wide spread of values for both aspartate residues; and that BpMip Tyr⁸⁹ shows two conformations (red ovals), whereas BpMip Trp⁶⁶ and LpMip Tyr²⁰⁵ show a single conformer.

REFERENCES

- Fulton, K. F., Jackson, S. E. and Buckle, A. M. (2003) Energetic and structural analysis of the role of tryptophan 59 in FKBP12. *Biochemistry* **42**, 2364–2372
- Löw, C., Neumann, P., Tidow, H., Weininger, U., Haupt, C., Friedrich-Epler, B., Scholz, C., Stubbs, M. T. and Balbach, J. (2010) Crystal structure determination and functional characterization of the metallochaperone SlyD from *Thermus thermophilus*. *J. Mol. Biol.* **398**, 375–390
- Szep, S., Park, S., Boder, E. T., Van Duyne, G. D. and Saven, J. G. (2009) Structural coupling between FKBP12 and buried water. *Proteins* **74**, 603–611

Received 24 February 2011/13 May 2011; accepted 16 May 2011
Published as BJ Immediate Publication 16 May 2011, doi:10.1042/BJ20110345